Lab on a Chip

PAPER

View Article Online
View Journal | View Issue

Cite this: *Lab Chip*, 2023, **23**, 3106

Acrylic-based culture plate format perfusion device to establish liver endothelial–epithelial interface†

Dennis McDuffie,[a] Charles G. Alver,[a] Bhumi Suthar,[a] Madeline Helm,[a] David Oliver,[a] R. Alan Burgess,[b] David Barr,[b] Emmanuel Thomas*[bc] and Ashutosh Agarwal *[acd]

Microphysiological Systems (MPSs) or organs-on-chips, are microfluidic devices used to model human physiology *in vitro*. Polydimethylsiloxane (PDMS) is the most widely used material for organs-on-chips due to its established fabrication methods and biocompatibility properties. However, non-specific binding of small molecules limits PDMS for drug screening applications. Here, we designed a novel acrylic-based MPS to capture the physiological architecture that is observed universally in tissues across the body: the endothelial–epithelial interface (EEI). To reconstruct the EEI biology, we designed a membrane-based chip that features endothelial cells on the underside of the membrane exposed to mechanical shear from the path of media flow, and epithelial cells on the opposite side of the membrane protected from flow, as they are *in vivo*. We used a liver model with a hepatic progenitor cell line and human umbilical vein endothelial cells to assess the biological efficacy of the MPS. We computationally modeled the physics that govern the function of perfusion through the MPS. Empirically, efficacy was measured by comparing differentiation of the hepatic progenitor cells between the MPS and 2D culture conditions. We demonstrated that the MPS significantly improved hepatocyte differentiation, increased extracellular protein transport, and raised hepatocyte sensitivity to drug treatment. Our results strongly suggest that physiological perfusion has a profound effect on proper hepatocyte function, and the modular chip design motivates opportunities for future study of multi-organ interactions.

Received 3rd May 2023,
Accepted 6th June 2023

DOI: 10.1039/d3lc00382e

rsc.li/loc

Introduction

Microphysiological Systems (MPSs), colloquially termed organs-on-chips, are promising new tools for modeling physiological functions *in vitro*. MPSs provide an enhanced means of studying organ physiology, disease etiology, and tissue-scale responses to treatments through microfluidics. In contrast to traditional two-dimensional (2D) plate culture, MPSs offer the benefits of establishing a physiologically relevant microenvironment *in vitro*. Cells cultured in a physiomimetic microenvironment have demonstrated enhanced longevity, function, and the capacity to illicit more physiologically accurate responses to infections, treatments, and stimuli than in 2D plates.[1] MPSs seek to model different organ systems and biological phenomena.

In this study, we designed a novel MPS to capture physiological architecture that is observed universally in tissues across the body: the endothelial–epithelial interface (EEI). Every organ is vascularized with capillaries, which are lined with endothelial cells that regulate nutrient exchange with the surrounding epithelial tissue.[2] Deficiencies at this interface are caused by numerous common conditions including diabetes, metabolic syndrome, hypertension, and smoking. Endothelial dysfunction plays a significant role in the development of atherosclerosis, angiogenesis in cancer, vascular leakage, infectious diseases, and stroke.[3] The EEI is implicated extensively in multiple disease etiologies, rendering it an excellent target for MPS modeling.

MPSs have evolved rapidly over the past several years, propelled in part by the use of photolithography and PDMS, a biocompatible material that has been widely incorporated in microfluidic devices.[4,5] PDMS bears several key advantages for use in MPSs: low cytotoxicity, optical transparency, gas permeability, low cost, and ease of manufacturing.[6] However, PDMS has some significant pitfalls as a biological material, especially in the context of drug assessment: PDMS non-

[a] *Department of Biomedical Engineering, University of Miami, Coral Gables, FL, USA. E-mail: A.agarwal2@miami.edu; Tel: +1 305 243 8925*
[b] *Department of Pathology & Laboratory Medicine, Schiff Center for Liver Diseases, University of Miami Miller School of Medicine, Miami, FL, USA. E-mail: Ethomas1@med.miami.edu; Tel: +1 305 243 2895*
[c] *Sylvester Comprehensive Cancer Center, University of Miami Miller School of Medicine, USA*
[d] *Desai Sethi Urology Institute, University of Miami Miller School of Medicine, USA*
† Electronic supplementary information (ESI) available. See DOI: https://doi.org/10.1039/d3lc00382e

specifically binds small-molecules and leaches uncrosslinked oligomers.[7] As an alternative to PDMS, minimally-bioactive plastics provide the same advantages, but without PDMS's adsorptive properties. Poly(methyl methacrylate) (PMMA) is a transparent reusable thermoplastic amenable to custom machining for the purpose of developing microfluidic devices.[8] We have previously demonstrated the feasibility of multiple PMMA devices for the functional assessment of pancreatic islets, the establishment of an alveolar air–liquid interface, and the re-creation of a glomerular filtration barrier.[9,10] Fabricated from the same processes, we unveil yet another microfluidic device, developed for the purpose of reproducing an EEI.

Here, we introduce a novel higher-throughput plate-format organ-on-chip design that models the EEI. This open-well design fabricated from inert plastics features a standard 24-well culture plate form factor, with 8 identical microfluidic devices for higher throughout experimentation. Each chip's membrane-based endothelial–epithelial co-cultures are readily accessible and amenable to a multitude of assays. The design successfully recapitulates the EEI by co-culturing endothelial and epithelial cells on opposite sides of the membrane, in order to achieve a physiological spatial architecture, while still retaining the cells' capacity to engage in cell-signaling. Using a liver model, we demonstrated improved cell longevity and enhanced cellular function in our system as compared to traditional 2D plate culture. In the case of the liver, the MPS captures the biology of the liver acinus, the functional unit of the liver comprised of the liver sinusoid (capillary) and parenchymal tissue (hepatocytes). Similar to the liver's physiology, the capillary or endothelial chamber is exposed to perfusion while the parenchymal or epithelial chamber remains under static conditions. This capillary–parenchyma relationship is prevalent throughout the entire body, not just the liver, therefore this MPS is highly translatable to numerous tissues and organs.

Materials and methods

Platform design and fabrication

The design of the microfluidic device was developed in SOLIDWORKS 2020 3D CAD software (Dassault Systèmes, France). Chips were machined from clear PMMA slabs (McMaster-Carr, Elmhurst, IL) using an MDX-540 CNC milling machine (Roland, Japan). Chips were assembled from two distinct top (1/2 inch thickness) and bottom (1/8 inch thickness) pieces *via* bonding with acrylic cement (McMaster-Carr). The bonded slabs were laser-cut to the dimensions of a standard 24-well culture plate with a 30 W CO_2 laser engraver (Epilog Laser, Golden, CO). On the top piece each of the 24 wells was milled to 15.62 mm in diameter, equivalent to those from a 24-well plate. The chip's 16 identical inlet/outlet ports were designed to be compatible to with mini male Luer-locks (ChipShop, Germany), which connect peristaltic tubing to the outlet. Each inlet/outlet well was milled at 2.67 mm in depth around the port holes, which were 2.81 mm in diameter and milled through the entire slab at a 1.72 degree inward draft angle. The chip's 8 culture wells were designed to house 13 mm diameter, 0.4 μm pore, circular PET membranes (Sterlitech, Kent, WA) for cell culture. The top side of the membrane had 132.7 mm^2 of cell culture surface area, while the bottom side of the membrane, once installed into the device well, had 0.95 mm^2 of cell culture surface area. The culture wells themselves were milled at 7.17 mm in depth around, and an 11 mm hole was drilled through the middle of the well to complete the membrane housing. The bottom slab featured 8 independent channels that aligned with the through-cut holes from the top slab. Channels were 40 mm in length, 2.5 mm in depth, and 2 mm in width through the narrowest section, but connected on both sides to a circular area beneath the culture well that was also 11 mm in diameter. 2 circular areas at each end of the channel 2.54 mm in diameter interfaced with the inlet and outlet ports from the top slab. Custom well casings with 3 mm holes to thread tubing through were also laser-cut from PMMA.

Computational modeling

Finite element modeling (FEM) analysis was performed using COMSOL Multiphysics 5.0 software (COMSOL Inc. Sweden). A 3D model of one individual channel was imported into COMSOL from Solidworks as a parasolid. The Free and Porous Media Flow physics module was used to solve for velocity and pressure fields of laminar flow through the perfusion channel. Fluid flow was modeled as the incompressible of flow water, governed by the Navier–Stokes equation. Flow rate was assigned as an outflow value at 40 μL min^{-1} to match the empirical value. A gravitational volume force was applied across the entire system. The perfusion channel in the model was separated from the culture well by a porous membrane. The Brinkman equation modeled flow across the membrane. Permeability of the membrane was calculated based on assumptions necessary to apply Hagen–Poiseuille's law for fluid flow, Ohm's law for electrical current flow, and Darcy's law for a fluid flow through a porous medium.[11] By assuming each pore is a cylindrical pipe, the permeability value (k) can be calculated as a function of pore radius through the given equation:

$$k = \frac{\pi \rho R^4}{8}$$

where (ρ) is pore density and R is pore radius. Even though the membrane acts as a barrier, the porous nature of the membrane allows for the model to incorporate static fluidic pressures from the culture well, that balance the static fluidic pressure from the fluid reservoir tower, which is technically connected to the entire channel. The offsetting hydrostatic pressures that allow the culture well and reservoir to reach an equilibrium are defined by the equation:

$$P = \rho g h$$

where the pressure (P) is proportional only to the height of the fluid (h) given that the fluid density (ρ) and gravitational constant (g) are constant in this system. A stationary solver determined the steady-state solution for velocity and pressure fields. Shear stress (τ) was also determined in different cut planes in the well, and is modeled by Newton's Law:

$$\tau = \gamma\eta$$

where (γ) is shear rate and (η) is fluid viscosity.

Albumin transport was modeled as a 28 day time-dependent study. The Transport of Diluted Species module was used to model albumin transport. A known value for the diffusion coefficient of albumin in water was used,[12] and the diffusion coefficient of albumin through the membrane was calculated using a derivation of Fick's first law, given by the equation:

$$D_{\text{ieffective}} = \frac{\varepsilon}{\tau} D_{\text{i}}$$

$D_{\text{ieffective}}$ is the effective diffusion coefficient through a porous medium, D_{i} is the diffusion coefficient of albumin in water, ε is the porosity of the membrane, and τ is tortuosity. Given the previous assumption that the pores are straight cylindrical pipes, τ is equal to 1. Albumin production was modeled as a reaction originating at the top surface of the membrane. The reaction rate was selected based on the knowledge that normal albumin turnover in the body is ~25 days,[13] and normal albumin concentration in the body is between 35 and 50 g L^{-1}.[14] Given that albumin concentration in the MPS starts at 0, the reaction rate of albumin in the MPS was originally set such that it reached a maximum concentration of 40 g L^{-1} at 25 days. However, the concentration of albumin in the body is dependent on albumin production from an average liver that is ~1500 g (ref. 15) with an average hepatocyte concentration of 116 × 10^6 hepatocytes/gram[16] into 5 liters of blood in the body,[17] equating to 1.914 pg per hour of albumin production from a single hepatocyte. Albumin production in the MPS was scaled to account for the 100 000 hepatocytes/well, equating to a final value of 191 ng per hour. In the perfusion model, the multi-physics module was applied to combine the physics from both the Free and Porous Media Flow module and the Transport of Diluted Species module to incorporate the constant flow and recycling of media. The outlet of the model was defined as an outflow port, and the inlet of the model was assigned an inflow flux value equal to the average concentration at the outlet port. To calculate the distribution of albumin throughout the model, the albumin in the channel was reported as a percentage of the total albumin in the MPS. To estimate the amount of albumin in the channel, an average channel concentration value was calculated by measuring the concentration at 5 evenly space points across the channel, at a cross-section 1 mm above the bottom surface of the channel. Each value was adjusted by a coefficient corresponding to the width of the channel at that point. The albumin concentration in the culture chamber was measured at a cross-section 2 mm above the cell layer surface at the center of the well. A total albumin value was calculated by multiplying the culture well value concentration by the volume of the well, then the average channel concentration value by the volume of the channel, and adding the two together. Computationally modeled albumin totals were calculated at 7, 14, 21, and 28 days.

Preparation of chips and 2D plates

Prior to use for experimentation, the chips and their components were sterilized by soaking the assembled chip in 10% bleach for 10 minutes, followed by 70% ethanol for 10 minutes, and finally UV-irradiation for 30 minutes while dry. Luer-locks and tubing were rinsed with ethanol and sterilized *via* autoclaving. 1 Luer-lock for each channel was inserted into each outlet well, each inlet in the reservoir wells remained open. Membranes arrived sterile and were only exposed under a biosafety cabinet. 2D 48-well plates were coated for at least one hour with rat tail collagen type I (100 μg mL^{-1} collagen in 150 μL of PBS) (Corning, Corning, NY). Collagen was removed and wells were washed with PBS. Individual membranes were placed into separate wells of a 24-well plate and each was coated with collagen using the same process (100 μg mL^{-1} in 300 μL of PBS). After coating, membranes were dried and anchored in the culture well using a silicone adhesive (McMaster-Carr, Part #7651A51).

Endothelial cell culture and seeding

Membranes were seeded first with either primary human umbilical vein endothelial cells (HUVECs) (Lonza, Switzerland) for HepaRG co-culture, or primary liver sinusoidal endothelial cells (LSECs) for primary human hepatocyte (PHH) co-culture (ScienCell, Carlsbad, CA). HUVECs were cultured on collagen-coated flasks and LSECs were cultured on fibronectin-coated flasks. Both endothelial cell types were cultured in complete EGM-2 (EGM-2 supplement pack includes FCS, epidermal growth factor, basic fibroblast growth factor, insulin-like growth factor, vascular endothelial growth factor 165, ascorbic acid, heparin, and hydrocortisone) (PromoCell, Germany) supplemented with 1% penicillin/streptomycin (P/S) (ThermoFisher, Waltham, MA), and fed with fresh medium every 48 hours. Once reaching confluence, cells were detached with phenol red free TrypLE (ThermoFisher), centrifuged for 5 minutes at 300*g*, and resuspended at a concentration of 1 million cells per mL. 2D 48-well plate wells were seeded at a density of 50 000 cells per well. In chip conditions, each channel was filled with suspension *via* syringe with 500 μL of cell suspension. Chips were then inverted and placed in the incubator for 2 hours to allow cells to attach. After 2 hours, chips were returned to their normal orientation, and each microfluidic channel was supplemented with 1 mL of medium in its culture well plus 1

mL of medium in its reservoir well, and placed in the incubator overnight.

Epithelial cell culture and seeding

HepaRG hepatocellular carcinoma derived cell line hepatocytes (ThermoFisher) were cultured on tissue-culture flasks in William's base medium supplemented with HepaRG Maintenance Medium Supplement (includes DMSO) (ThermoFisher), 1% Glutamax, and 1% P/S, and fed with fresh medium weekly. HepaRGs were cultured in monoculture (mono) and co-culture (cc) with HUVECs in 2D. HepaRGs do not require an extracellular matrix coating. One day after seeding HUVECs, HepaRGs were detached with phenol red free TrypLE (ThermoFisher), centrifuged for 5 minutes at 300*g*, and resuspended in 10 mL of medium. Before seeding 2D co-cultures, EGM-2 media was removed from 2D wells previously seeded with HUVECs, and replaced with HepaRG media. Before seeding onto the chip membrane, EGM-2 medium was removed from every reservoir well and culture well, and replaced with 1 mL of HepaRG medium in each well. EGM-2 medium that remained in the microfluidic channels was replaced by attaching a syringe to the Luer-lock at the outlet, and draining the entirety of the HepaRG-medium-filled reservoir well into the channels. EGM-2 medium pulled from the channel into the syringe was discarded. After the reservoir wells were drained, they were replenished with 1 mL of HepaRG medium. 100 000 HepaRGs/well were then seeded into the chip culture wells opposite the HUVECs. 2D monoculture and 2D co-culture wells were also seeded with 100 000 HepaRGs/well.

Cryopreserved primary human hepatocytes (ThermoFisher) were thawed in primary hepatocyte plating medium (ThermoFisher), seeded onto collagen coated plates and membranes, then cultured in dHCGM media (PhoenixBio, Hiroshima, Japan) supplemented with heat-inactivated FBS (ThermoFisher) after 4 hours in plating medium. Seeding density depended on culture platform because unlike HepaRGs, PHHs do not actively replicate. MPS culture wells were seeded with 400 000 cells/well because even though the viable cell culture surface area is similar to a 48-well plate, the entire well opening is the size of a 24-well plate. 48-well plates were seeded with 200 000 cells/well. 4 hours after seeding when the plating medium was replaced by dHCGM in the culture well, EGM-2 medium that remained in the reservoir well and microfluidic channel was replaced with dHCGM as well. EGM-2 medium was removed from each reservoir well and replaced with 1 mL of dHCGM. EGM-2 medium that remained in the microfluidic channels was replaced by attaching a syringe to the Luer-lock at the outlet, and draining the entirety of the dHCGM-medium-filled reservoir well into the channels. EGM-2 medium pulled from the channel into the syringe was discarded. After the reservoir wells were drained, they were replenished with 1 mL of dHCGM.

Perfusion

One day after seeding hepatocytes, the chip was equipped with peristaltic tubing to begin perfusion. For each MPS undergoing perfusion, one 0.64 mm ID peristaltic tube (Cole-Parmer, Vernon Hills, IL) was attached to the Luer-lock on end, and the other end was threaded through the 3 mm hole in the well-casing and into the reservoir well. Each tube was connected to the pump, and perfusion began by pulling media from the channel up through the Luer-lock and tubing, and dripping back into the reservoir well at a rate of 40 μL min^{-1}. Only half of the MPS channels on the chip were subjected to perfusion, the other half served as static controls. Perfusion was maintained continuously for up to 4 weeks with full media changes twice per week. Static and 2D conditions were also maintained for up to 4 weeks with media changes twice per week.

CYP3A4 activity measurements

CYP3A4 activity was measured in live cells using a CYP P450-Glo™ assay specific to CYP3A4 (Promega, Madison, WI) according to manufacturer instructions. Because of small differences in cell culture surface are between the 48-well 2D condition (1.1 cm^2) and the chip membrane (1.33 cm^2), the same volume of media + luciferin-IPA was added to each well and CYP activity was measured as luminescence/cm^2 to account for differences in cell density. 24 hour rifampin (10 μM) (Alfa Aesar, Haverhill, MA) was used in some conditions to induce CYP3A4 activity.

LDH cytotoxicity assay

LDH released by cells in media was measure using the CyQUANT™ LDH Cytotoxicity Assay (ThermoFisher, Waltham, MA) according to manufacturer instructions. Media samples were collected every 7 days from each culture condition.

RT-qPCR

Transcriptional expressions of hepatic differentiation markers were measured *via* RT-PCR. Total RNA was extracted using the RNeasy Plus kit (Qiagen, Germany) according to manufacturer instructions. cDNA was synthesized using qScript cDNA SuperMix synthesis kit (Quantabio, Beverly, MA) according to manufacturer instructions. Primer-probe sets labeled with 6-FAM were used to quantify expression of albumin (Hs.PT.56a.1501965), CYP3A4 (Hs.PT.58.1272782), and HNF4A (Hs.PT.58.22303533) (IDT, Coralville, IA). Expression was normalized to 18S ribosomal RNA labeled with VIC (Applied Biosystems, Waltham, MA). Gene expression was quantified using the $2^{-\Delta\Delta Ct}$ method.

Immunofluorescent staining and imaging

When imaging HepaRGs, HUVECs were removed from the bottom side of the membrane by scraping, when imaging

HUVECs, HepaRGs were removed from the top side of the membrane by scraping. This removal facilitated location of the proper focal plane. The remaining cells were fixed in 4% paraformaldehyde for 20 minutes while membranes remained in the MPS. The membranes were then cut out of the well, removed from the chip, and placed into a new 24-well plate where they were permeabilized with 0.3% Triton-X for 10 minutes and blocked for an hour in 1% BSA + 1% goat serum. The membranes were incubated with primary antibody solutions (diluted 1 : 100) at 4 °C overnight. For HepaRGs, an albumin primary antibody was used (A6684, Sigma-Aldrich, St. Louis, MO), for HUVECs a ZO-1 primary antibody was used (5406, Cell Signaling, Danvers, MA). The following day, membranes were incubated with secondary antibodies (diluted 1 : 1000) for 90 minutes at room temperature. HepaRGs used an anti-mouse secondary (A32723, ThermoFisher), HUVECs used an anti-rabbit secondary (A21206, ThermoFisher). Membranes were washed with PBS and mounted on to slides using ProLong™ Gold antifade mounting medium (Life Technologies, Carlsbad, CA). Images were acquired with a Zeiss LSM confocal microscope.

Albumin ELISA

HepaRG albumin production in the media was measured with a human albumin ELISA kit (Bethyl Labs, Montgomery, TX). Media samples were collected every 7 days from each culture condition. For the MPS conditions, media was collected from both the culture and reservoir wells. Samples were diluted 1 : 250 and assayed with the kit according to manufacturer instructions.

Statistical analysis

Statistical significance was determined using one-way ANOVA and Tukey's *post hoc* test for data in Fig. 4, 6A, S2 and S3.† A two-way ANOVA and Šídák's test for multiple comparisons was used for data in Fig. 6B, 7 and S1.† An alpha level of 0.05 was used to determine significance. Error bars represent standard deviation.

Results

Design, fabrication, and assembly of an endothelial–epithelial interface chip

Design/fabrication. The design of our MPS aims to capture the biological architecture of the liver acinus, the functional unit of the liver comprised of the liver sinusoid (capillary) and parenchymal tissue (hepatocytes). Similar to the liver's physiology, the capillary or endothelial chamber is exposed to perfusion while the parenchymal or epithelial chamber remains under static conditions (Fig. 1). The system was designed to replicate a standard 24-well culture plate, and features the same well diameters and spacing. A model of the platform was developed using 3D computer-aided design (CAD) and then machined using a CNC milling machine. The plate is comprised of two PMMA slabs, laser cut to the dimensions of a 24-well culture plate, and irreversibly bonded with acrylic cement. The bottom slab has 8 distinct channel engravements, each spanning lengthwise between 3 wells, and the top piece consists of 24 wells with through-cuts, aligned appropriately with the channels (Fig. 2B). Of the 24 well openings, 16 are reservoir/outlet wells with 2.8 mm diameter through-cut holes, and 8 are culture wells with 11 mm diameter through-cut hole. In total, there are 8 identical

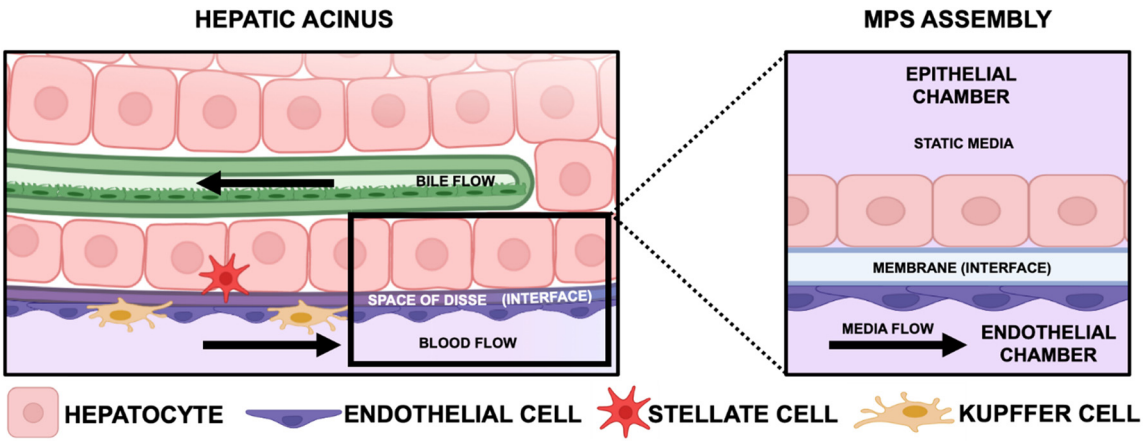

Fig. 1 Hepatic acinus. The hepatic acinus is the smallest functional unit of the liver, comprised of the hepatic sinusoid blood vessel and its surrounding epithelium. The acinus has four resident cell types: hepatocytes are the parenchymal cells that carry-out the majority of the liver's functions, endothelial cells line the sinusoid and perform cell-signaling and barrier functions, Kupffer cells are the resident macrophages, and stellate cells are quiescent in a healthy liver but are activated and modulate inflammation in a diseased liver. For the purpose of constructing an EEI with a liver model, only endothelial cells and hepatocytes were used in the MPS assembly. The MPS features a membrane that mimics the EEI with endothelial cells and hepatocytes cultured on its opposing sides. Media is perfused beneath the endothelial cells in the endothelial chamber, but remains stagnant on the hepatocytes in the epithelial chamber. *Figure made in biorender*.

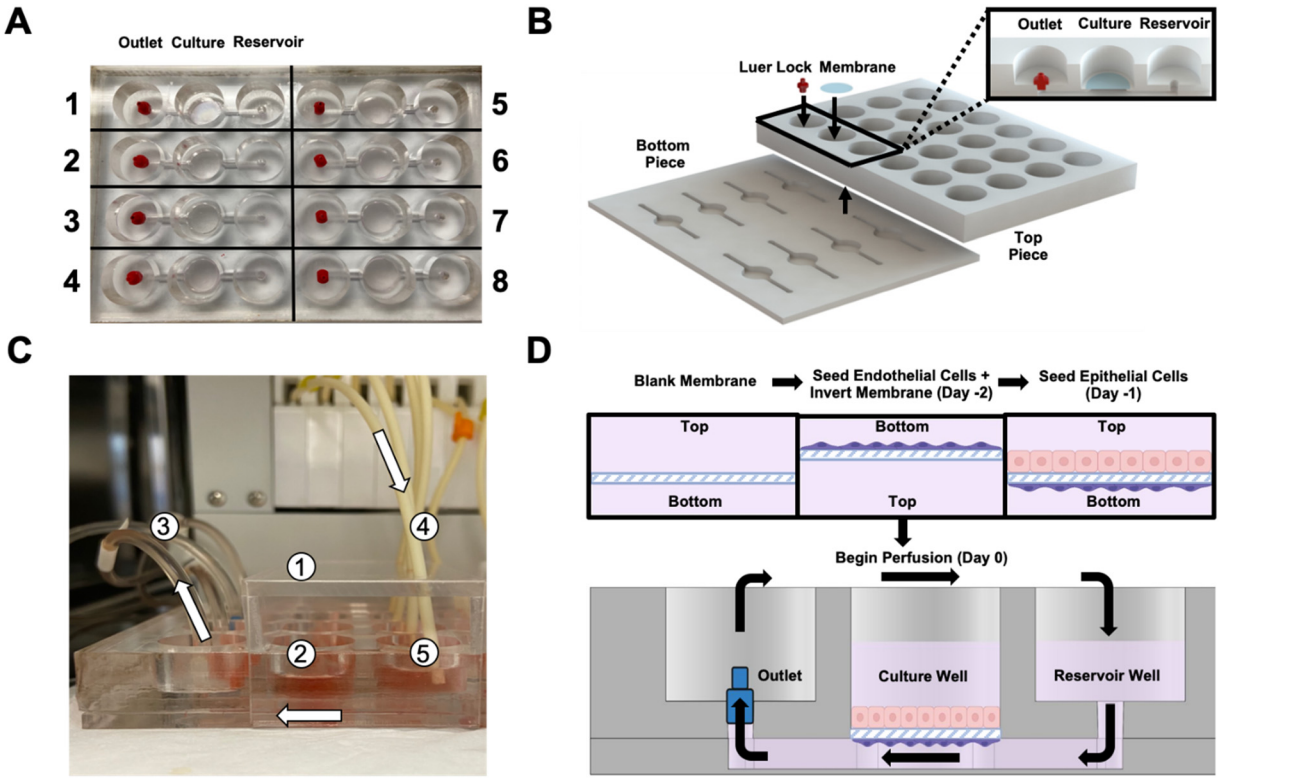

Fig. 2 Chip design, assembly, and use. The chip was designed to resemble a standard 24-well culture plate. It is comprised of 8 reservoir wells, 8 culture wells, and 8 outlet wells (A). The chip features four main components: a bottom piece with 8 channel engravings for the 8 individual MPSs, a top piece with through-cuts to connect the wells to the channels, Luer-locks in each outlet well to connect peristaltic tubing to the channel, and membranes in each culture well where cells are seeded (B). An acrylic well-casing (1 protects the culture (2 and reservoir wells (5. When connected to a pump, media is recirculated through peristaltic tubing (4 that pulls media from the reservoir and channel, through the outlet (3, and drips back into the reservoir (5 (C). Cell seeding begins two days before perfusion, starting first with seeding endothelial cells on the underside of the membrane, followed by seeding hepatocytes on the upper side of the membrane the next day, and finally starting perfusion the day after (D).

chips on a single plate (Fig. 2A). Protective well covers with tubing holes were also fabricated from PMMA (Fig. 2D).

Assembly. Reservoir and outlet wells were machined identically, but reservoir wells were filled with media, while outlet wells were plugged with plastic Luer-locks that connect microfluidic tubing to the chip (Fig. 2A and B). The culture wells housed removable PET membranes, which were bonded to a well lip using a silicone adhesive (Fig. 2B). The membranes served as substrates for endothelial–epithelial co-culture. In the body, endothelial cells line blood vessels and are mechanically stimulated by shear forces induced by blood flow. Conversely, epithelial cells are protected from the path of blood flow, but still participate in nutrient exchange and cell-signaling with the endothelium.[18,19]

To capture this physiology, endothelial and epithelial cells were cultured on opposite sides of the same membrane. The chip features two distinct chambers: an endothelial chamber for media perfusion to simulate blood flow (bottom channel), and an epithelial chamber which is removed from the flow path, but still allows for transport across the membrane (upper well) (Fig. 2D). 2 days prior to beginning experimentation, endothelial cell suspension was seeded on the bottom side of the membrane in their own media. The next day, hepatocytes were seeded onto the upper side of the membrane, and the media in the entire system was changed to hepatocyte media. The day after, perfusion began *via* peristaltic pumping: pulling media down from the reservoir well, across the channel, through the tubing, and recycling back into the reservoir (Fig. 2C and D). In the chip's lower chamber, peristaltic pump-driven perfusion promotes nutrient transport and physiological shear at the endothelial surface. In the upper chamber, passive diffusion across the membrane permits nutrient exchange and cellular cross-talk without exposing epithelial tissue to potentially caustic shear.

Modeling flow mechanics

Media flow through the MPSs was modeled using COMSOL multi-physics software. As demonstrated by the model, the MPS reaches an equilibrium, governed by static fluidic pressure, when the height of the media in the culture well and reservoir wells is equal. If the height of the media in one well drops but stays the same in the other, the pressure will be greater in the higher well, and the volume in the higher well will fall as the volume in the lower well rises until an equilibrium is re-established (Fig. 3A). Under these equilibrium conditions, flow of media through the chip is generated primarily *via* pump through the lower chamber.

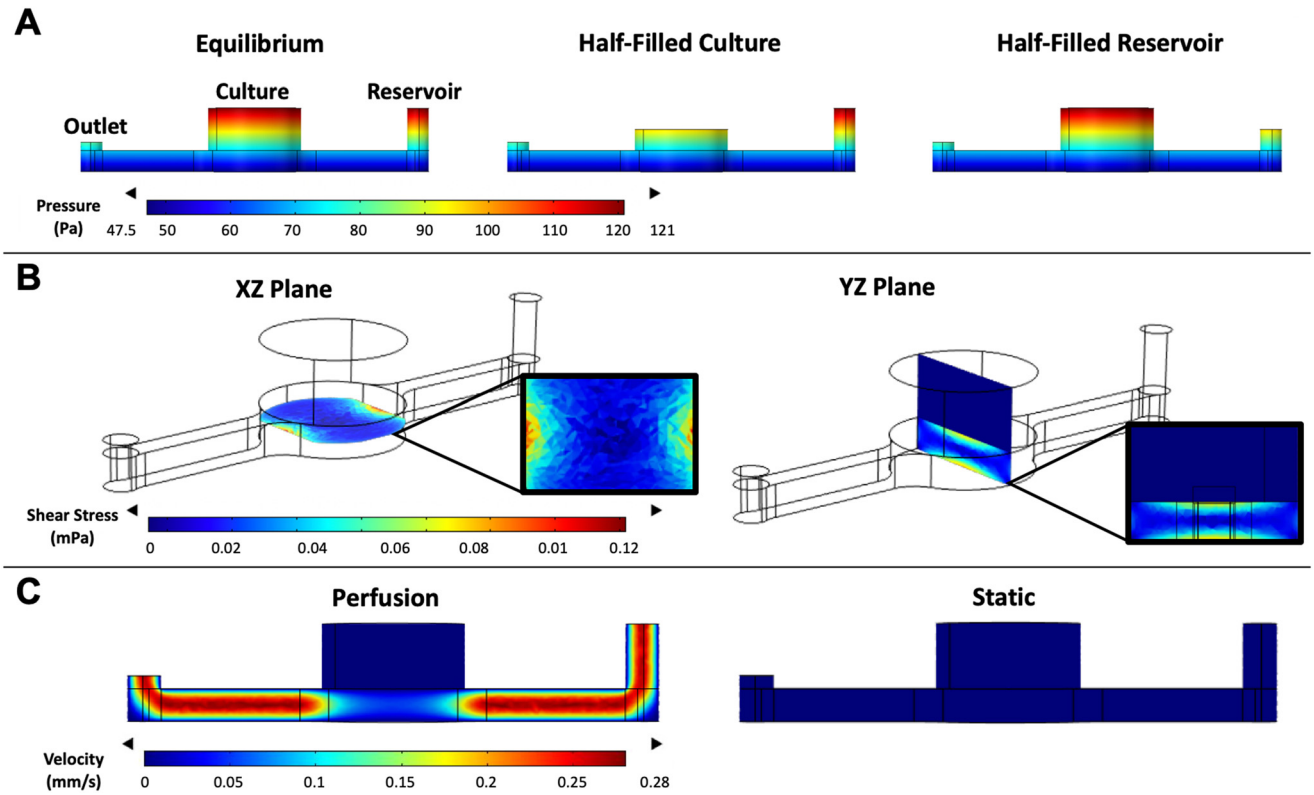

Fig. 3 Modeling flow. Each MPS in the chip reaches an equilibrium that is regulated by hydrostatic pressure. By creating artificial scenarios where the volume in the culture well is lower, or the volume in the reservoir well is lower, the system deviates from its equilibrium and will self-regulate the volumes in the two wells until equilibrium is reestablished (A). Physiological shear has a documented benefit on the functionality of endothelial cells. Here shear is modeled in both the *XZ* and *YZ* planes, and is maximized near the center of the well and at the endothelial surface where it is most desirable (B). The velocity profile through the MPS during perfusion shows how fluid moves faster through the narrow ends of the channel, and slows through the wide center of the well. Under static conditions, velocity is zero, and does not induce relevant shear at the endothelial surface (C).

The flow of media induces fluidic shear, which is maximized near the center of the channel at the edge of the membrane, and at the channel and membrane surfaces (Fig. 3B). Maximizing shear at the membrane surface where the endothelial cells are attached is critical for their mechanical stimulation. Fluid velocity through the channel is laminar and greatest at the two narrow ends of the channel. Flow is slowest through the center of the well where the cross-sectional area expands. In the static simulation, flow is essentially non-existent (Fig. 3C).

Differentiating HepaRG cells on the chip

To assess the biological functionality of the EEI chip, the HepaRG hepatic progenitor cell line was selected to model epithelial tissue, and human umbilical vein endothelial cells (HUVECs) were selected to model endothelial tissue. HepaRGs were selected because they are commercially available and offer the capacity to be differentiated into more functionally mature hepatocytes. HUVECs were selected as a non-specific endothelial cell source, which can be translated to numerous organ system models. A perfusion co-culture proved to significantly improve HepaRG differentiation as compared to monoculture (Fig. S1†). Fluid flow rates (Fig. S2†) and media combinations for the co-culture (Fig. S3†) were also optimized experimentally for 7 days. Using the optimized conditions of a HUVEC–HepaRG co-culture with all HepaRG media flowed at 40 μL min^{-1}, the viability of both of the HUVECs and the HepaRGs was demonstrated for up to 28 days *via* immunofluorescent imaging. All cells were stained with nuclei-targeting DAPI and F-actin-targeting phalloidin. HepaRGs were stained with albumin, a hepatocyte-specific protein, and HUVECs were stained with ZO-1, an endothelial cell-junction protein (Fig. 4A). Although endothelial and epithelial cells have a mutualistic relationship, the benefits provided to the epithelial cells by the endothelial cells were of greater interest. As a result, only the hepatocytes were assayed for differentiation markers including albumin, CYP3A4, and HNF4A. Each culture condition was assayed at 1, 2, and 4 weeks. The EEI MPS perfusion condition both upregulated and maintained higher expression of hepatocyte differentiation markers as compared to 2D monoculture, 2D co-culture, and the static MPS co-culture. The differences in expression of albumin and HNF4A were minimal after only a week, but became significant after 2 and 4 weeks. For CYP3A4 however, the

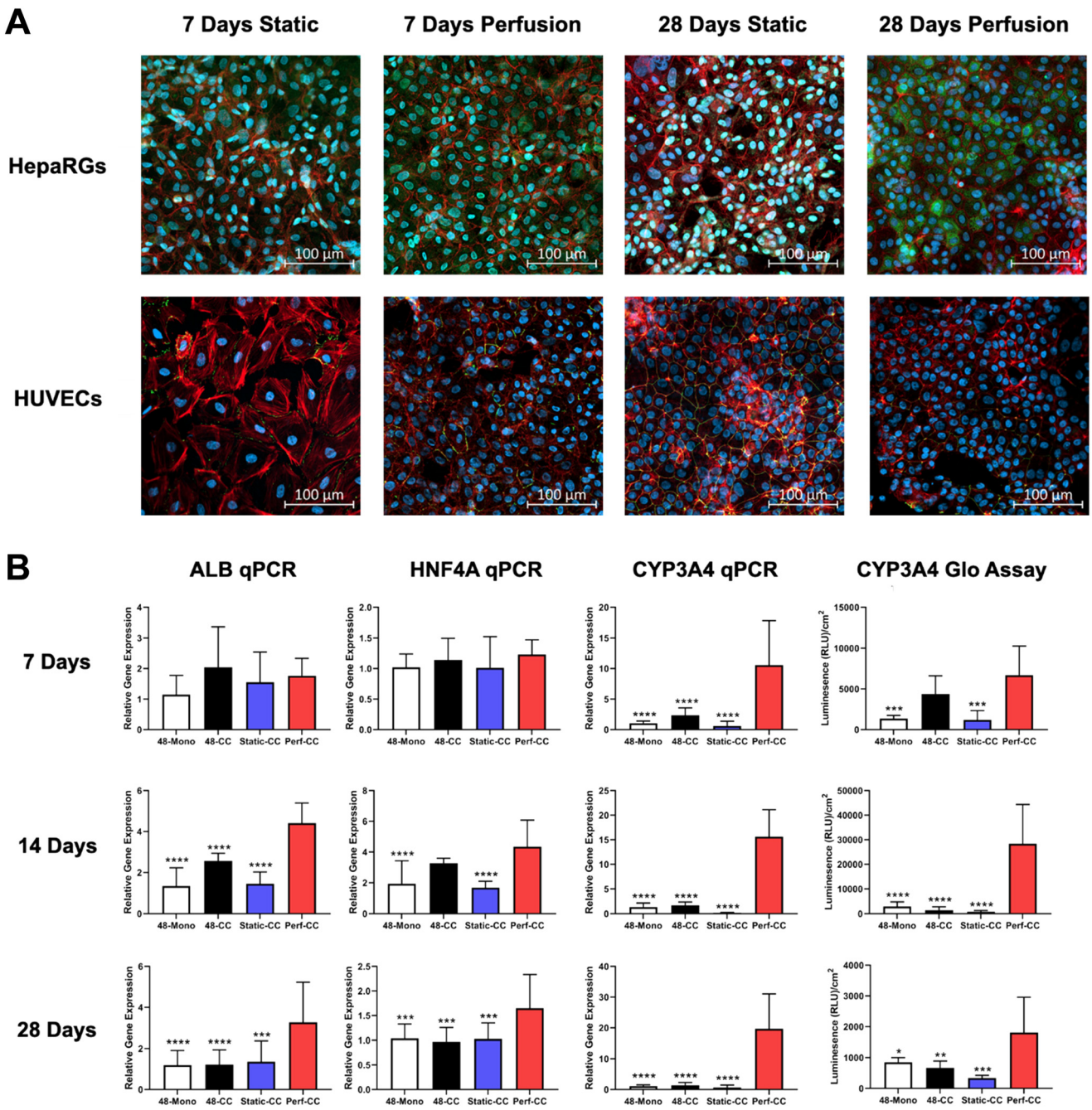

Fig. 4 Cell viability and differentiation. Immunofluorescent images of the top (HepaRGs) and bottom (HUVECs) of the membranes were taken for both static and perfusion conditions at 7 and 28 days and demonstrate sustained viability of both cell types over the course of 28 days. Blue = DAPI, red = phalloidin, green HepaRGs = albumin, green HUVECs = ZO-1 (A). Hepatocyte differentiation marker expression was assessed at 7, 14, and 28 days by PCR and CYP3A4 glo assay for each culture condition: 2D 48-well monoculture (Mono), 2D 48-well co-culture (CC), static MPS CC, and perfusion MPS CC. Across all three markers, the perfusion MPS increased hepatocyte expression of differentiation markers and maintained significantly higher expression levels over 28 days relative to the other culture conditions. Statistical significance was determined using one-way ANOVA and Tukey's *post hoc* test (n = 8) (B). The values on each graph represent the mean ± SD. Significance is given with respect to the perfusion MPS co-culture condition *$p < 0.05$, **$p < 0.01$, ***$p < 0.001$, ****$p < 0.0001$.

perfusion MPS condition significantly upregulated its expression and activity after 7 days and maintained high levels the entirety of the 28 days. When compared to the static MPS condition, perfusion appears to have the most pronounced effect in the upregulation of CYP3A4 (Fig. 4B). This result demonstrates that the platform can be used for both short and long-term culture, indicating its broad applications for disease models with different chronologies, and capacity to assess acute and chronic response to drug compounds.

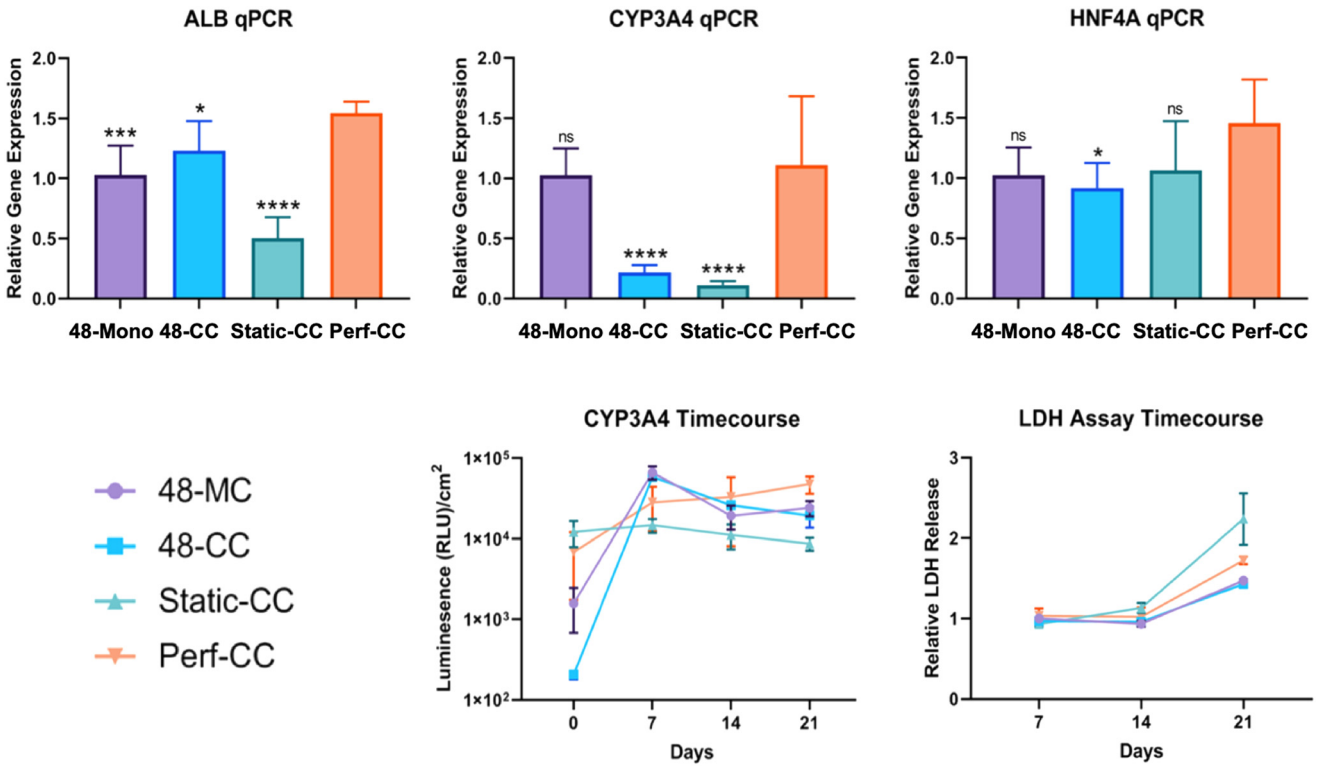

Fig. 5 Three week PHH culture condition comparison. PHHs were cultured on the MPS and in 2D for 21 days. The MPS condition was either not significantly different, or demonstrated improved function over all other culture conditions. The values on each graph represent the mean ± SD. Statistical significance was determined using one-way ANOVA and Tukey's *post hoc* test ($n = 4$). Significance is given with respect to the perfusion MPS co-culture condition *$p < 0.05$, **$p < 0.01$, ***$p < 0.001$, ****$p < 0$.

Maintaining PHH functionality on the chip

In addition to differentiating HepaRGs with this platform, we were able to combat loss of functionality in PHHs over three weeks and demonstrate improved PHH function in the MPS as compared to 2D culture. Unlike HepaRGs, PHHs cannot be further differentiated, but dedifferentiation can be prevented, which was our goal for culturing PHHs on the platform. We established the same culture conditions that were used for the HepaRGs, though this time replacing HUVECs from our co-cultures with hepatic-specific LSECs. Using qPCR, we assayed for the same three functional markers that we assayed for in the HepaRGs (Albumin, CYP3A4, HNF4A), all of which are downregulated as PHHs dedifferentiate. We also recorded LDH activity weekly over three weeks to assess loss of viability over time (Fig. 5). In total, we found that the MPS both improves and better maintains primary hepatocyte function as compared to 2D culture and static chip culture over the course of three weeks.

Using perfusion to increase albumin production and transport

Albumin is secreted by hepatocytes, but it plays a critical role throughout the body by regulating plasma oncotic pressure, transporting ligands, and scavenging potentially toxic plasma constituents.[20,21] Therefore, it is imperative that albumin not only be produced by the liver, but also be transported away from the liver through the bloodstream to carry out its functions. Here we show that perfusion not only bolsters albumin production from hepatocytes, but also increases the transport of albumin away from the liver. To demonstrate this, albumin secreted into the media was assayed from each culture condition every 7 days for 28 days. Media was changed in each condition twice a week for the entirety of the experiment, so the albumin measured every 7 days was the total that had accumulated in the media over the prior 3 days. Each culture condition was seeded with 100 000 hepatocytes/well, but the 2.5 mL of media in each MPS chip was 5 times that of the 0.5 mL in each 2D well. To adjust for this difference in volume, albumin is plotted as a total in nanogram (ng) rather than a concentration. Furthermore, because albumin is only produced in the culture well of the MPS, it was not prudent to assume that the concentration of albumin in the culture well was the same as the concentration of albumin in the reservoir and channel. Therefore, to calculate the total amount of albumin in the MPS, samples were taken from both the culture well and the reservoir well. The culture well sample concentration was multiplied by 1, representing the 1 mL of media in the culture well, and the reservoir sample was multiplied by 1.5, representing the 1.5 mL of media in the reservoir well and channel. These two values were combined to calculate the total albumin/chip. Albumin levels in the media fluctuated over the course of the 28 days, but the perfusion MPS

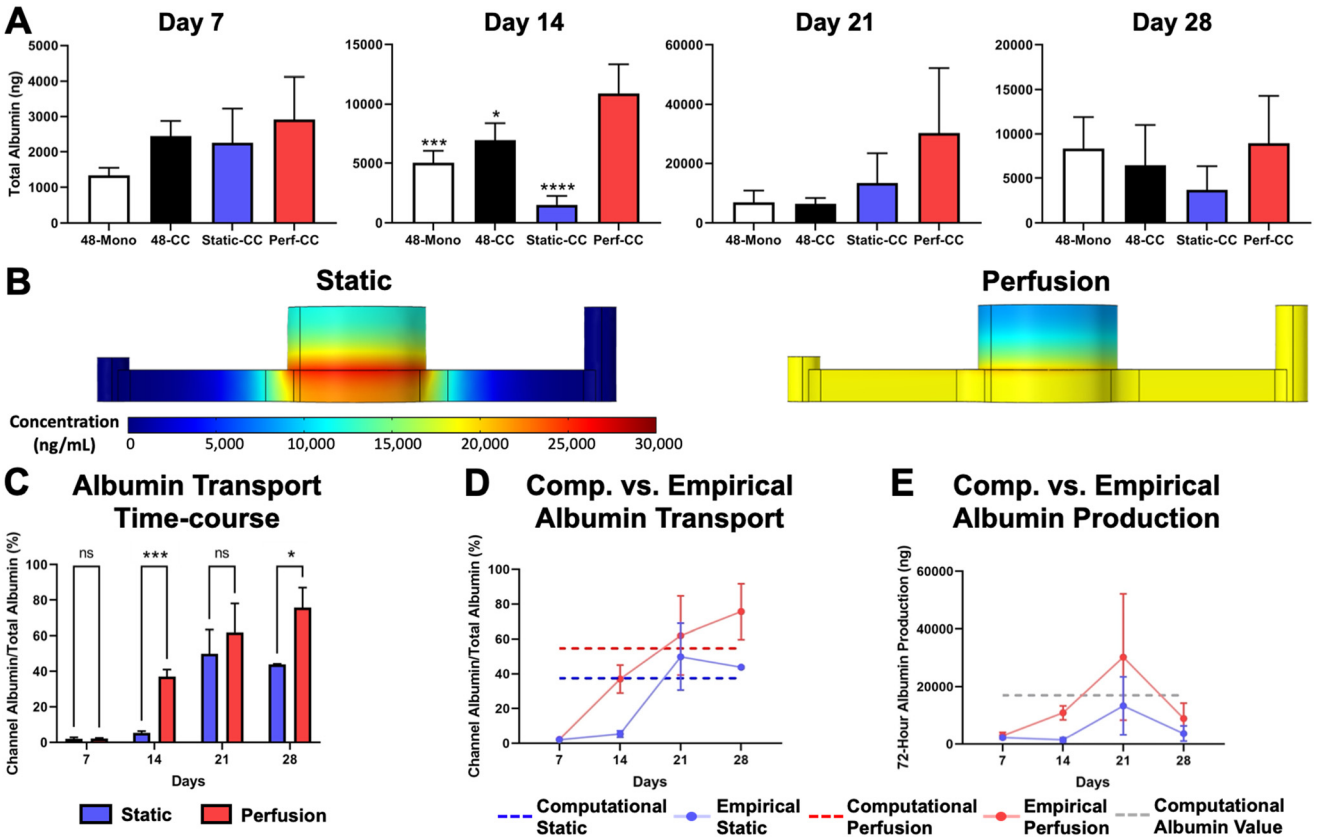

Fig. 6 Albumin production and transport. Total albumin in the media was measured every 7 days for 28 days in each culture condition: 2D 48-well monoculture, 2D 48-well co-culture, static MPS co-culture, and perfusion MPS co-culture. These values represented the albumin that was produced over the prior 3 days since the last media change. At each time point, the perfusion MPS media produced the most total albumin. Statistical significance was determined using one-way ANOVA and Tukey's *post hoc* test (n = 4) (A). The accumulation of albumin in the MPS over a 3 day period was also modeled computationally for both static and perfusion MPS conditions. The static condition formed a concentration gradient based on proximity to the hepatocyte layer: albumin concentration decreased further from the hepatocytes. In the perfusion model, albumin concentration was greatest near the membrane surface, but was overall more evenly distributed throughout the channel and culture well than the static condition (B). Albumin transport from the culture well to the channel was measured by plotting the albumin measured in the channel and reservoir as a percentage of the total albumin in the MPS over time for both static and perfusion conditions. Albumin transport increased over time and was significantly higher in the perfusion condition. Statistical significance was determined using two-way ANOVA and Šídák's multiple comparison test (n = 4) (C). These empirical *in vitro* data from each time point were plotted against the computational model value of albumin distribution after 3 day of culture. The perfusion condition increased transport in both the empirical and computational models, but the empirical model stimulated transport of albumin into the channel even more so than was possible computationally (D). The total albumin production values for the static and perfusion conditions from (A) were plotted against the computed production value over 3 days. Both the static and perfusion computational models were represented by a single total production value because both were assigned the same reaction rate. The computational values were much higher than the empirical values, but this is to be expected given that the computational reaction rates were defined based on albumin production *in vivo*, and did not account for media changes that occurred *in vitro* (E). The values on each graph represent the mean ± SD. Significance is given with respect to the perfusion MPS co-culture condition *$p < 0.05$, **$p < 0.01$, ***$p < 0.001$, ****$p < 0.0001$.

condition consistently had the highest production, and was significantly higher than the 3 other conditions at 14 days (Fig. 6A). Albumin secretion and distribution through the MPS was also modeled computationally with COMSOL as static and perfusion simulations using physiological albumin production values as described in the methods. Albumin production was only modeled up to 3 days, given the assumption that all albumin was removed entirely from the system during each media change. The static simulation showed albumin was highest near the center of the well, but formed a proximity-based concentration gradient that decreased further from the membrane. The perfusion simulation showed a similar high concentration near the membrane surface, but exhibited a more uniform distribution of albumin throughout the channel due to the increased albumin transport caused by flow of media. Both computational models were assigned the same reaction rate, so the total albumin produced over 3 days was the exact same in both the static and perfusion conditions (Fig. 6B). To illustrate albumin transport from the culture well into the channel and reservoir well, albumin outside of the culture well in the channel and reservoir was plotted as a percentage of the total albumin from each MPS for every time point. The perfusion condition had a greater percentage of its total albumin in the channel and reservoir than the static condition at every time point, and was significantly higher at

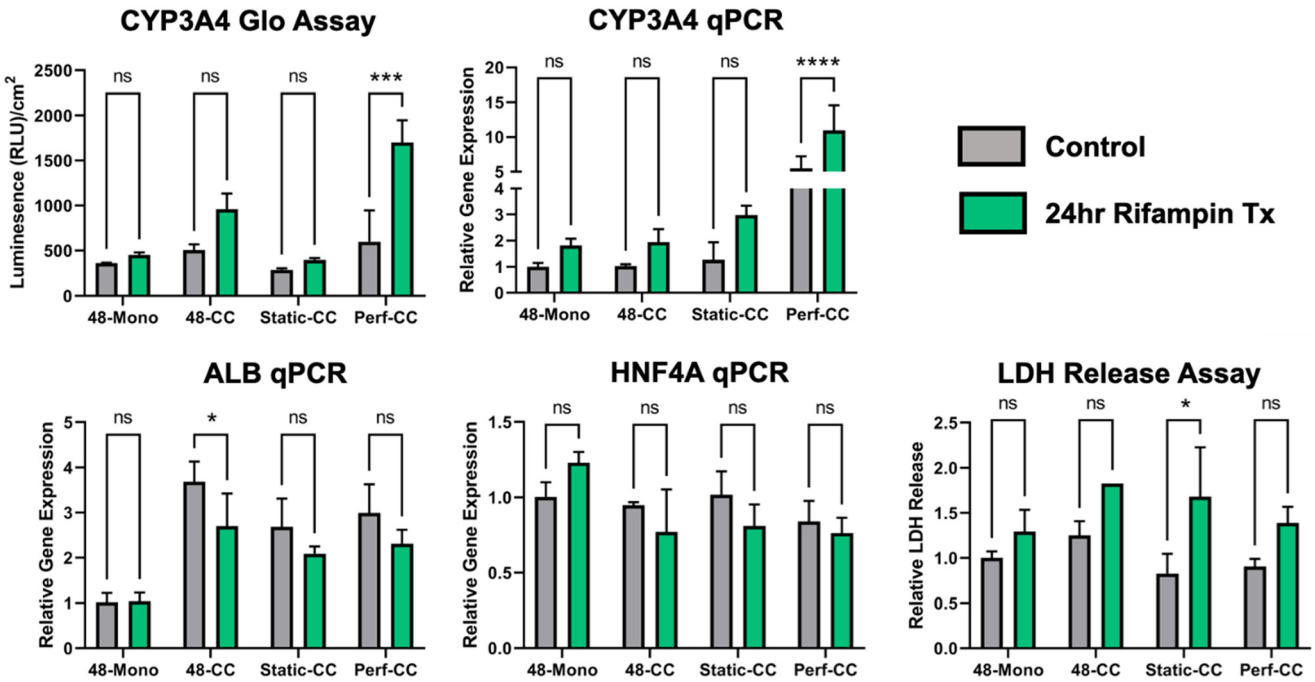

Fig. 7 Rifampin sensitivity. Hepatocyte sensitivity to rifampin was assessed across culture conditions: 2D 48-well monoculture, 2D 48-well co-culture, static MPS co-culture, and perfusion MPS co-culture. Albumin, HNF4A, and LDH release were also assayed to ensure that the rifampin did not have significant toxic or dedifferentiating effects on the hepatocytes. An anticipated upregulation of CYP3A4 expression was observed in the treatment *vs.* the control across all culture conditions, but only in the perfusion MPS condition was there a statistically significant increase in the treatment compared to the control. The values on each graph represent the mean ± SD. Statistical significance was determined using two-way ANOVA and Šídák's multiple comparison test ($n = 4$) *$p < 0.05$, **$p < 0.01$, ***$p < 0.001$, ****$p < 0.0001$.

14 and 28 days. Albumin transport also continuously increased in the perfusion condition over the 28 days. This increase in transport, in spite of regular media changes, indicates that transport may also be driven by improvements to hepatocyte phenotypic function. (Fig. 6C). These empirical *in vitro* data were plotted against transport values generated from the computational simulations. Concentration values were taken at the same points in the culture and reservoir wells of the computational models 2 mm from the cell surface in the center of the culture well, and 2 mm below the cell surface at 5 different points across the MPS channel, and total albumin values were calculated by multiplying concentration values by volume to convert to mass. As depicted in Fig. 6B, the perfusion simulation demonstrated a higher degree of transport than the static simulation. *In vitro*, albumin from the static condition increased gradually until day 14, had a rapid increase between days 14 and 21, and dipped after day 21. The perfusion condition resembles a logarithmic curve: it increased rapidly from day 7 to 14, then continued to increase but at a slower rate. Albumin transport from the static *in vitro* model converged near the computational static model value by day 28, but the perfusion *in vitro* model surpassed the computational perfusion simulation by day 21 and continued to climb at day 28. While the end point of the *in vitro* static condition was close to the computed value, the *in vitro* perfusion condition substantially outperformed its computational counterpart. The computational model is unable to account for the differentiative phenotypic effects that mechanical stimulation may have on the hepatocytes' albumin production, and the transport effects that the resulting concentration gradient may cause biologically. Increased production as a result of mechanical stimulation may explain the discrepancy between computational and *in vitro* data in the perfusion condition (Fig. 6D). A comparison of total albumin production in the system between static and perfusion conditions was plotted for both the computational and *in vitro* models. Both computational models were represented by a single 72 hour total production value for each time point, because their albumin production rate inputs were identical. This rate was defined using clinical data for albumin production in a healthy person. The empirical perfusion value at 21 days surpassed that of the computational model, before dropping at day 28. The empirical static value followed a similar trajectory, closely approaching the computational value at 21 days, then exhibiting the same decrease at 28 days. This comparison between the *in vitro* MPS albumin assay and clinical data is far from perfect given that we modeled albumin production with a cancerous cell line and cannot assume that all albumin is leaving the system during each media change. However, the fact that the empirical values oscillated just above and below the computational values indicated that the hepatocytes in the MPS were producing albumin near physiological levels (Fig. 6D).

Drug sensitivity response

The perfusion MPS excelled in its ability to upregulate CYP3A4 expression and activity. CYP3A4 comprises 15–20% of CYP enzymes in the liver and is responsible for metabolizing an estimated 50% of all drugs.[22] Because CYP3A4 is so heavily implicated in drug metabolism, we tested whether the MPS's capacity to upregulate its baseline expression and activity would translate to an increased response in activity and expression when targeted with rifampin, a known CYP3A4 inducer. Each condition was cultured for 6 days, then media was changed, and each well was replenished with either 10 μM rifampin diluted in media, or media without rifampin for 24 hours. Samples were assayed on day 7 for CYP3A4 activity and expression as well as expression of albumin, and HNF4A to ensure the rifampin did not have a significant dedifferentiating effect. LDH release in the media was also assayed to ensure that the rifampin did not have a significant cytotoxic effect. Upregulation of CYP3A4 activity and expression was observed in every culture condition, but was only significantly upregulated between the treatment and control in the perfusion MPS condition, indicating that the MPS provided increased sensitivity to the hepatocytes' drug response. Hepatocytes from the perfusion MPS did not exhibit a significant decrease in albumin or HNF4A expression, nor did they demonstrate a significant decrease in viability (Fig. 7).

Discussion

The simplicity of the chip design is intentional such that it can be readily applied to mimic a variety of different biological systems, and is not exclusive to the liver. Fundamentally, all vascularized tissues have an endothelium and epithelium, and finding a generic way to simulate this architecture *in vitro* may provide a more systemic perspective to the study of disease, drug response, and general physiology of different tissues in the body as opposed to studying tissues in isolation. Moreover, the minimally-bioactive properties of acrylic ameliorate issues in PDMS devices with non-specific protein binding, particularly relevant in drug study.[7,8] Secluding all cell culture to a removable membrane insert allows the MPS to be reused, and makes for easy assaying, fluorescent imaging, and cell-specific ECM coating. The reusability of this platform makes it highly translational to commercial use, in an effort to ameliorate the immense costs required of single-use platforms. The design is limited in its capacity for live-cell imaging, but the open-well format provides rapid access to media from the culture well and channel for easy sample collection and live-cell biochemical assays that are far more difficult to conduct in sealed MPS platforms. The open well format also subverts issues with media leaks and irretrievable bubbles that can be potentially catastrophic for an experiment, but are commonplace problems with sealed devices.

The internal reservoir well was implemented as a solution to problems with both media backflow that raised the volume of the culture well, and media draining that lowered the volume of the culture well. In a preliminary design iteration in which we used an external reservoir that was connected by tubing to both the inlets and outlets, we learned that the media volume in the culture well depended on reservoir volume height. Rather than perfectly adjusting the reservoir height to match the volume of the culture well, we built the reservoir well into the system of flow so that it would self-regulate the volumes of each well.

Using the liver to represent an EEI has clear utility given the need for improved modeling of drug response and disease pathogenesis in the liver. However, our selection of cell source to model the liver EEI was motivated by desire to create a generalizable platform that could be applied to any organ systems. HepaRGs were an appealing cell source because they are a readily available cell line, but also are progenitor cells that have the capacity to demonstrate increased functionality upon differentiation.[23] We were able to use this platform to push these cells towards this more differentiated state. Furthermore, HepaRG cells are contact-inhibited, and therefore amenable to the 4 week studies we conducted, without the concern of overgrowth that would come with other non-contact-inhibited cell lines. The HUVECs were selected because they are a generalizable endothelial cell source that can be applied to co-culture with a variety of tissues. Our goal was to show that HUVECs could provide a benefit as a cell type within our EEI platform.

To demonstrate that we could indeed apply this model to a specific organ system, we used primary hepatocytes along with their native LSECs. The HepaRG and PHH cultures served different purposes, because the HepaRGs proved that the chip could differentiate the cells towards a more functional hepatocyte phenotype, while the PHHs proved that the chip could better maintain a functional hepatocyte phenotype. Drug response studies are the most common application of liver-on-chip platforms, and are typically conducted over short periods of time where loss of hepatocyte function is less of a concern. However, the proven ability of this platform to maintain hepatocyte function for long-term culture expands opportunities for different applications, including more biologically relevant time-dependent drug studies and chronic disease pathogenesis. Using both a HepaRG–HUVEC co-culture and a PHH–LSEC co-culture, we effectively demonstrated that the EEI platform improves and maintains hepatocyte function better than in other culture conditions, thereby providing greater opportunities for biologically-relevant *in vitro* assessments.

Though we hypothesized that shear induced from media perfusion would have a substantial impact on differentiation of HepaRGs and maintenance of PHH function based on similar work,[24,25] the degree to which the perfusion condition outperformed the static MPS condition exceeded expectations. Based on knowledge that prolonged exposure to fluid shear stress improves endothelial function,[26–31] and

COMSOL simulations that indicate shear through the well is highest near the membrane bottom surface, we hypothesize that the shear induced by perfusion is a major contributing mechanism to the differentiation of HepaRGs and maintenance of functional PHHs.

In addition to shear induction, media perfusion also played a crucial role in albumin transport from the culture well into the channel. By treating the culture well as the tissue, and channel and reservoir as the bloodstream, we observed that perfusion aids in carrying albumin away from its production site as it would in the body, and this transport increases with increasing time in culture. This finding is intriguing not only because it demonstrates that flow limits tissues from festering in its own secretions and minimizes osmotic limits of albumin accumulation, but also because it illustrates how we were able to study the impact of a protein secreted from the liver on a tissue downstream or *vice versa* in a way that would not be possible without perfusion. Because the design of the system is generalizable to host different epithelial chambers connected by a single endothelial chamber, we can see how this platform would serve as a generic EEI that allows for a multi-organ on chip design to be formed. Our production process has already allowed us to design and create a chip that connects 4 separate culture wells flanked by two inlet outlet wells using the same 24-well plate format (Fig. S4†). Recognizing the impact of perfusion on protein transport has opened up a wide array of future directions in which we can combine different organ systems with the liver culture, and screen the downstream effects of drugs and treatments to the liver on off-target organs.

While screening off-target drug effects is a viable future direction, we observed increased on-target drug sensitivity in hepatocytes when treating them with rifampin. This finding demonstrates the potential of this platform for liver-specific drug toxicity studies that could potentially show more pronounced effects in the perfusion MPS than in typical 2D drug toxicity platforms. Our observation of significant CYP3A4 upregulation in only the perfusion condition indicates that by upregulating the baseline expression and activity of hepatic enzymes specific to the metabolization of a drug, we can see a more pronounced effect of that drug on the enzymes that metabolize it. This could provide more insight into the mechanism by which a drug is metabolized, as well as amplifying any toxic effects that may not otherwise be observed in traditional 2D culture.

Conclusion

We designed a novel, multi-throughput, acrylic-based microphysiological system to capture the physiology of the endothelial–epithelial interface, and used a liver model to demonstrate its biological functionality. By combing physiomimetic endothelial cell and hepatocyte co-culture with mechanically-stimulating media perfusion, we were able to promote differentiation and improve the functionality of the hepatic progenitor HepaRG cell line, and better maintain primary hepatocyte function, as compared to traditional culture techniques. The generic design of this platform allows for seamless a translation from the liver to numerous different biological applications. The EEI is pervasive throughout the human body and modeling this architecture in the liver is a preliminary step towards recapitulating this physiology in a variety of organ systems and eventually linking them. Similarly, modeling defective EEIs may be useful in the study of cancer metastasis and other afflictions that result from leaky vasculature or deficient cell barriers. We hope that this platform is a valuable tool for the study of physiological barrier functions.

Abbreviations

MPS	Microphysiological system
PDMS	Polydimethylsiloxane
EEI	Endothelial–epithelial interface
2D	Two-dimensional
PMMA	Polymethyl methacrylate
CAD	Computer-automated design
FEM	Finite element modeling
HUVEC	Human umbilical vein endothelial cell
CNC	Computer-numerical control

Author contributions

Dennis McDuffie: conceptualization, methodology, investigation, formal analysis, visualization, writing. R. Alan Burgess, Madeline Helm, Charles G. Alver, Bhumi Suthar, David Barr: investigation. Emmanuel Thomas, Ashutosh Agarwal: conceptualization, resources, supervision, writing.

Conflicts of interest

The authors have no conflicts of interest to disclose.

Acknowledgements

This work was supported by Sylvester Comprehensive Cancer Center Transdisciplinary Pilot award (parent grant P30CA240139) to ET and AA, NIH-NIGMS grant R35GM124915 to ET, and NIDDK-supported Human Islet Research Network (HIRN; **https://hirnetwork.org/**; UH3DK122638) to AA.

References

1 S. N. Bhatia and D. E. Ingber, *Nat. Biotechnol.*, 2014, **32**, 760–772.
2 B. Alberts, A. Johnson, J. Lewis, M. Raff, K. Roberts and P. Walter, *Molecular Biology of the Cell*, Garland Science, New York, 4th edn, 2022, Available from: **https://www.ncbi.nlm.nih.gov/books/NBK21054**.
3 P. Rajendran, T. Rengarajan, J. Thangavel, Y. Nishigaki, D. Sakthisekaran, G. Sethi and I. Nishigaki, *Int. J. Biol. Sci.*, 2013, **9**, 1057–1069.

4 K. M. Raj and S. Chakraborty, *J. Appl. Polym. Sci.*, 2020, **137**, 48958.
5 T. Fujii, *Microelectron. Eng.*, 2002, **61–62**, 907–914.
6 K. Ren, J. Zhou and H. Wu, *Acc. Chem. Res.*, 2013, **46**, 2396–2406.
7 B. J. van Meer, H. de Vries, K. S. A. Firth, J. van Weerd, L. G. J. Tertoolen, H. B. J. Karperien, P. Jonkheijm, C. Denning, A. P. IJzerman and C. L. Mummery, *Biochem. Biophys. Res. Commun.*, 2017, **482**, 323–328.
8 C. Matellan and A. E. del Río Hernández, *Sci. Rep.*, 2018, **8**, 6971.
9 M. Ishahak, J. Hill, Q. Amin, L. Wubker, A. Hernandez, A. Mitrofanova, A. Sloan, A. Fornoni and A. Agarwal, *Front. Bioeng. Biotechnol.*, 2020, **8**, DOI: **10.3389/fbioe.2020.581163**.
10 G. Lenguito, D. Chaimov, J. R. Weitz, R. Rodriguez-Diaz, S. A. K. Rawal, A. Tamayo-Garcia, A. Caicedo, C. L. Stabler, P. Buchwald and A. Agarwal, *Lab Chip*, 2017, **17**, 772–781.
11 C. G. Sip, N. Bhattacharjee and A. Folch, *Lab Chip*, 2014, **14**, 302–314.
12 Diffusion coefficient of human serum albumin – Generic – BNID 100612, **https://bionumbers.hms.harvard.edu/bionumber.aspx?s=n&v=7&id=100612**, (accessed December 9, 2021).
13 D. G. Levitt and M. D. Levitt, *Int. J. Gen. Med.*, 2016, **9**, 229–255.
14 N. Mclntyre and S. Rosalki, in *Scientific Foundations of Biochemistry in Clinical Practice*, ed. D. L. Williams and V. Marks, Butterworth-Heinemann, 2nd edn, 1994, pp. 383–398.
15 D. K. Molina and V. J. M. DiMaio, *Am. J. Forensic Med. Pathol.*, 2012, **33**, 368–372.
16 Z. E. Wilson, A. Rostami-Hodjegan, J. L. Burn, A. Tooley, J. Boyle, S. W. Ellis and G. T. Tucker, *Br. J. Clin. Pharmacol.*, 2003, **56**, 433–440.
17 R. Sharma and S. Sharma, in *StatPearls*, StatPearls Publishing, Treasure Island (FL), 2021.
18 K. Kaarj and J.-Y. Yoon, *Micromachines*, 2019, **10**, 700.
19 A. Varone, J. K. Nguyen, L. Leng, R. Barrile, J. Sliz, C. Lucchesi, N. Wen, A. Gravanis, G. A. Hamilton, K. C. Karalis and C. D. Hinojosa, *Biomaterials*, 2021, **275**, 120957.
20 P. B. Soeters and P. W. de Leeuw, in *Reciprocal Translation Between Pathophysiology and Practice in Health and Disease*, ed. P. B. Soeters and P. W. de Leeuw, Academic Press, 2021, pp. 151–165.
21 R. N. Moman, N. Gupta and M. Varacallo, in *StatPearls*, StatPearls Publishing, Treasure Island (FL), 2021.
22 R. G. Tirona and R. B. Kim, in *Clinical and Translational Science*, ed. D. Robertson and G. H. Williams, Academic Press, 2nd edn, 2017, pp. 365–388.
23 D. McDuffie, D. Barr, A. Agarwal and E. Thomas, *Front. Microbiol.*, 2022, **13**, DOI: **10.3389/fmicb.2022.999366**.
24 M. Boul, N. Benzoubir, A. Messina, R. Ghasemi, I. B. Mosbah, J.-C. Duclos-Vallée, A. Dubart-Kupperschmitt and B. Le Pioufle, *Sci. Rep.*, 2021, **11**, 14075.
25 K. M. Bircsak, R. DeBiasio, M. Miedel, A. Alsebahi, R. Reddinger, A. Saleh, T. Shun, L. A. Vernetti and A. Gough, *Toxicology*, 2021, **450**, 152667.
26 B. Wojciak-Stothard and A. J. Ridley, *J. Cell Biol.*, 2003, **161**, 429–439.
27 P. F. Davies, *J. Vasc. Res.*, 1997, **34**, 208–211.
28 N. Azuma, N. Akasaka, H. Kito, M. Ikeda, V. Gahtan, T. Sasajima and B. E. Sumpio, *Am. J. Physiol.*, 2001, **280**, H189–H197.
29 J. H. Hoger, V. I. Ilyin, S. Forsyth and A. Hoger, *Proc. Natl. Acad. Sci. U. S. A.*, 2002, **99**, 7780–7785.
30 M. Noris, M. Morigi, R. Donadelli, S. Aiello, M. Foppolo, M. Todeschini, S. Orisio, G. Remuzzi and A. Remuzzi, *Circ. Res.*, 1995, **76**, 536–543.
31 F. Kabirian, G. Amoabediny, N. Haghighipour, N. Salehi-Nik and B. Zandieh-Doulabi, *J. Biomed. Mater. Res., Part A*, 2015, **103**, 1231–1237.